JOURNAL OF SPACECRAFT AND ROCKETS
Vol. 44, No. 4, July–August 2007

Quasi-Static Optics-Based Surface Control of an In-Plane Actuated Membrane Mirror

Michael J. Shepherd,* Richard G. Cobb,† Gina A. Peterson,‡ and Anthony N. Palazotto§
Air Force Institute of Technology, Wright–Patterson AFB, Ohio 45433

DOI: 10.2514/1.24847

Future space telescopes may use large-diameter, flexible, lightweight membrane mirrors to overcome current launch weight and packaging limitations. In-plane actuated tensioned membrane mirrors may be a possible solution to maintaining the precise surface required of a telescope mirror. For this experiment a 0.127-m diam in-plane actuated deformable tensioned membrane mirror was constructed and tested. The research presented herein implements control algorithms based on the results of a nonlinear finite element MSC.Nastran model. The control method used a least-squares approach to create an influence function matrix which was implemented as a proportional plus integral controller. Precision shaping of the test article's mirror surface, expressed in terms of a Zernike coefficient basis set obtained from an optics-based Shack–Hartmann wave front sensor, was demonstrated in a series of quasi-static closed-loop control tests. Micron-level sinusoidal control inputs representing the defocus Zernike coefficient were successfully tracked with an average absolute accuracy of 0.16 μm. For multimode tracking, commanded tip, tilt, and defocus modes were tracked with an absolute average error of 0.14, 0.09, and 0.18 μm, respectively, indicating that increasing the dimension of the control system did not significantly degrade its performance. This experimental demonstration illustrates the use of optics-based precision surface control for in-plane actuated membrane mirrors, however, significant technological challenges still exist which may impede the use of this technology for large space-based telescope applications.

Nomenclature

$[A]$	=	system static matrix, QF^{-1}
$[c^E]$	=	stiffness matrix, FL^{-2}
D	=	plate stiffness, FL
$\{E\}$	=	electric field vector, FQ^{-1}
F	=	fundamental force unit
H	=	indicator function, $(-)$
$[K]$	=	actuator gain matrix, FQ^{-1}
L	=	fundamental length unit
M	=	fundamental mass unit
M_p	=	piezoelectric strength, F
N	=	edge tension function, FL^{-1}
Q	=	fundamental charge unit
R	=	radius of deformable mirror, L
r	=	radial coordinate, L
$\{S\}$	=	strain vector, $(-)$
t	=	actuator thickness, L
$\{V\}$	=	voltage, FLQ^{-1}
$\{v\}$	=	vector of applied voltage to each actuator, FQ^{-1}
$[X]$	=	applied actuation voltage matrix, FLQ^{-1}
$\{z\}$	=	vector of Zernike coefficients, L
$\{z_{\text{desired}}\}$	=	desired vector of Zernike coefficients, L
$\{z_e\}$	=	error signal vector of Zernike coefficients, L
$\{z_{\text{measured}}\}$	=	measured vector of Zernike coefficients, L
$\{\alpha\}$	=	thermal expansion coefficient vector, Θ^{-1}
ΔT	=	change in temperature, Θ
ε	=	tension asymmetry orientation constant, $(-)$
Θ	=	fundamental temperature unit
θ	=	azimuthal coordinate, $(-)$
κ	=	normalization scale factor, $(-)$
λ	=	wavelength, L
$\{\tau\}$	=	stress vector, FL^{-2}
ϱ	=	tension asymmetry constant, FL^{-1}

Subscripts

0	=	initial
1, 2, 3	=	x, y, z directions

Presented as Paper 2229 at the 47th AIAA/ASME/ASCE/AHS/ASC Structures, Structural Dynamics, and Materials Conference, Newport, Rhode Island, 1–4 May 2006; received 2 June 2006; revision received 21 February 2007; accepted for publication 24 February 2007.

*Lieutenant Colonel, USAF, Department of Aeronautics and Astronautics. AIAA Student Member.

†Assistant Professor, Department of Aeronautics and Astronautics. AIAA Senior Member.

‡Captain, USAF, Department of Aeronautics and Astronautics.

§Professor, Department of Aeronautics and Astronautics. AIAA Fellow.

I. Introduction

THE use of lightweight, large-diameter membrane mirrors as the primary aperture for space telescopes is proposed for both Earth surveillance and astronomical applications. The experiment design described herein had its roots in inflatable lenticular designs by the U.S. Air Force Research Laboratory [1]. The concept originated by Bekey [2] in 1999, however, with a formation flying 25-m diam aperture and large focal length (and correspondingly low radius of curvature) primary mirror as its central feature is another possible geometry that avoids the complexities of a gas-filled lenticular. This nonpressurized membrane mirror is the class of mirror envisioned for this study. An artist's conception of such a system is depicted in Fig. 1. As envisioned, the primary membrane mirror is attached to a rigid circular boundary, and localized precision surface control of the primary mirror is achieved through in-plane actuation.

Researchers at the Air Force Institute of Technology (AFIT) and NASA have proposed using in-plane actuated deformable mirrors to control the surface metrology of the primary mirror, as reported later. To date, there has not been a comprehensive effort to experimentally demonstrate the validity of this control methodology. It is the purpose of this work to report the experimental efforts to demonstrate quasi-static control of the surface of an in-plane actuated tensioned membrane deformable mirror as measured at the micron level. This experiment is representative of the type of surface control scheme that may be expected of larger scale membrane mirrors for space telescopes.

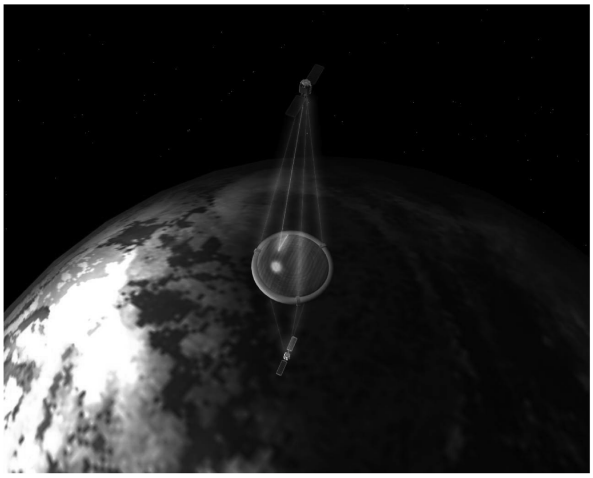

Fig. 1 Artist's conception of the large membrane mirror space telescope.

This objective was accomplished by applying known nonlinear finite element techniques to create a model of the membrane structure. The in-plane piezoelectric forcing was introduced using the familiar piezoelectric-thermal analogy. The modeling results were incorporated in a traditional controller using proportional plus integral control. The controller was implemented experimentally on AFIT's deformable mirror test bed. The controller was used to track commanded slowly varying low-order Zernike modes measured in real time by a Shack–Hartmann wave front sensor.

II. Background

Membrane deformable mirrors for space and near-space applications remain a subject of intense interest for the military and civilian research communities. The performance of a telescope is fundamentally governed by the size of its primary mirror, but diametrically opposed to that goal is the need to create tightly packaged lightweight payloads for use with the supporting launch vehicles. Thus, membrane mirror research seeks to create, deploy, shape, and control large-diameter lightweight mirrors capable of being compactly stored before their deployment. A significant enabling technology is the use of embedded in-plane piezoelectric actuators to activate the structure. The actuated membrane mirror could therefore potentially counter optical aberrations in the beam path, improve the optical quality (or smoothness) of the deployed reflector surface, and minimize the effects of mechanical disturbances. An experimental effort to achieve open and closed-loop quasi-static surface control on this class of mirror is the primary effort of this research. For the work described herein *quasi static* is defined as a control bandwidth which is significantly below the physical system vibratory dynamics.

Deformable lightweight mirrors for optical applications are of three basic types characterized by their actuating mechanism: conventional, edge controlled, and in plane actuated. Each type is discussed briefly below.

Conventional mirrors employ actuators acting perpendicular to the backing surface of the mirror and generally require a stiffened substructure affixed to the mirror. Electrostatic mirrors such as the work presented by Moore et al. [3] are a subset of this category. Large conventional mirrors for space applications must overcome the weight penalty imposed from the stiffened substructure.

Edge-controlled, or equivalently boundary-controlled, lightweight mirrors rely on actuators along the periphery of the mirror structure to induce surface changes. The edge-controlled mirror suffers some performance penalty in achieving conjugate surfaces for optical control [4,5], but recent research by Lindler and Flint indicates promising advances lie ahead in this field [6]. Further demonstrations in precision edge control of inflated lenticular mirrors have been reported by Patrick et al. [7] where the desired initial shape is achieved by depositing a varied stress coating onto the reflective polymer to alter the local mechanical properties of the membrane. It is our opinion that edge control may be essential to prevent wrinkling and to achieve the baseline shape of a deformable mirror. Fine high spatial frequency surface control, however, is not well suited to edge-controlled membrane mirrors where the lack of bending (or plate) stiffness limits the controllability of boundary actuators. A mechanism that acts directly on the surface of the mirror would not be limited by this constraint.

In-plane actuated deformable mirrors rely on piezoelectric (or other electrostrictive or magnetostrictive) actuators to produce an applied moment directly to the face of the mirror. The moment is created due to a strain offset from, and parallel to, the structure's neutral axis thus imparting a surface curvature. When compared to conventional and boundary control mirrors the moment actuation characteristic of in-plane actuated mirrors gives rise to the potential for greater spatial resolution as recognized in such works as that by Hubbard and Burke [8]. The term *in-plane actuation* was chosen in lieu of the term *bimorph corrector* mirrors as used by Tyson [9] to describe this class of deformable mirror, due to the fact that the term bimorph is overly precise. The class may be further subdivided into three types based on the actuation mechanism, as shown in Fig. 2 and described later.

The *unimorph* deformable mirror is constructed with piezoelectric actuators bonded to the mirror backing. Each piezoelectric actuator expands or contracts, and based upon its distance from the composite structure's neutral axis, induces a surface curvature. The regions of actuation generally correspond to the electrode pattern of the positive electrodes. The term unimorph was suggested for this type of actuator configuration by Adelman in 1977 [10]. Unimorph construction is the most simple construction technique for in-plane actuators.

Similar to the unimorph, the bimorph also employs piezoelectric actuators governed by an electrode pattern, but in pairs at each actuator location. The piezopair act in opposite directions to produce a local curvature. As the mirror coating is reduced the system approaches a symmetric structure which is easier to model. A drawback of this design technique, however, is the manufacturing complexity created by the requirement to apply opposite voltages on each piezoelectric component of the piezopair. Some caution must be used when searching the early literature as the term bimorph was used in 1979 by Itek Corporation to describe a class of mirrors that were deformed by piezobeam cantilevers forcing on push rods connected to the mirror in a conventional actuator configuration [11]. *Printthrough* has been a significant challenge in the fabrication process for in-plane actuated mirrors [12]. Printthrough occurs when a discrete actuator pattern causes a mechanical irregularity that results in a distortion on the reflecting surface. A bimorph mirror with two sets of actuating electrodes (one of which is necessarily closer to the reflective surface) is at a higher risk of printthrough than unimorph construction where the electrode pattern is only on the surface opposite the reflecting surface.

The *discrete* in-plane actuator is characterized by fixed blocks affixed to the backing side of the continuous mirror. A piezoactuator pushes laterally on the blocks which pivot on a central axis. The surface therefore deforms in segments. This type of in-plane actuated mirror is generally best suited to microelectromechanical systems such as those proposed by Yang [13] and is not discussed further here.

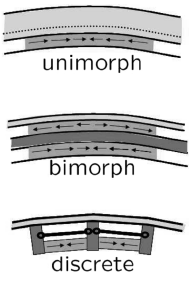

Fig. 2 In-plane actuated deformable mirror types.

To summarize, the significant advantages of in-plane actuation for space applications versus conventional and edge-controlled mirrors are the weight savings due to the lack of requirement for a stiff supporting structure and a potential increased stroke and spatial resolution of the deformable mirror surface. In fact, Açikmeşe et al. [14], the designers of the proposed NASA L2 Earth atmosphere experiment, espoused the benefits of using in-plane polyvinylidene fluoride (PVDF) actuators for surface metrology of the large-diameter primary mirror but noted further improvements in understanding were required to implement hardware control. Of the available in-plane actuation methods unimorph actuation is further explored herein due to its simplicity, lesser susceptibility to printthrough, and ease in manufacturing.

The modeling of an in-plane actuated structure is well understood —a comprehensive derivation of the governing equations were presented in the text by Nayfeh and Pai [15]. In its simplest form the governing analytic linearized equation for the out-of-plane displacement (w) of an isotropic plate membrane (a structure with both plate stiffness D and membrane tension N) undergoing piezoelectric actuation of uniform strength (M_p) over a region defined by an indicator function (H) of value one within the region and zero outside of the region is [15]

$$D\nabla^4 w(r,\theta) - N\nabla^2 w(r,\theta) = M_p \nabla^2 H(r,\theta) \tag{1}$$

where r is the radial coordinate from $0 \le r \le R$, θ is the azimuthal coordinate, and ∇^2 is the Laplacian operator which in cylindrical coordinates is

$$\nabla^2 = \frac{\partial^2}{\partial r^2} + \frac{1}{r}\frac{\partial}{\partial r} + \frac{1}{r^2}\frac{\partial^2}{\partial \theta^2}$$

Early deformable mirrors using in-plane actuation were primarily plate structures which effectively neglected membrane tension. They were designed for optical devices where weight was not a concern, plate stiffness was high, and development was sought primarily to exploit their curvature inducing advantage when compared to conventional mirrors [8,16]. Based on this historical precedence, attempts to model and experimentally verify results typically used only a deformable plate model. This was the case presented by researchers Sumali et al. [17] from the Sandia Laboratory which have recently demonstrated the in-plane actuation method for an 8 cm × 8 cm flat plate reflector with pinned corners.

For the space telescope problem envisioned, neglecting the membrane tension resulting from the supporting frame is not a valid assumption. This can be seen by nondimesionalizing the radial coordinate in Eq. (1). Letting $\hat{r} \equiv r/R$ yields

$$\frac{D}{R^2}\nabla^4 w(\hat{r},\theta) - N\nabla^2 w(\hat{r},\theta) = M_p \nabla^2 H(\hat{r},\theta) \tag{2}$$

From this simple scaling it may be seen that as the radius (R) increases in size and other material properties and parameters such as plate stiffness (D) and piezoelectric forcing (M_p) remain constant, the surface deflection w will be dominated increasingly by the preexisting membrane tension N. In almost every case it is foreseeable that a fixed edge structure would impart some level of intrinsic strain and, therefore, preexisting membrane tension that was neglected for smaller scale test articles as insignificant must be accounted for in larger scale systems such as a space telescope.

For a small-scale test article of equal thickness to be representative of a larger scale (larger radius) telescope it must have a much higher tension field than the plate stiffness term. To that end, an experimental demonstration of the ability to statically actuate a unimorph, in-plane actuated, tensioned membrane mirror was proposed by AFIT researchers Agnes and Wagner [12] and experimentally verified by Sobers et al. [18]. The mirror, the AFIT deformable mirror test bed, was a simplified flat, 2-D circular membrane versus the envisioned low radius of curvature 3-D paraboloidal surface for a space telescope. These previous works demonstrated open-loop static shaping, but efforts to model and experimentally control a mirror to submicron tolerances such as will be required for a future space telescope mission have not been attempted.

Solving the plate-membrane in-plane actuated system governing equations analytically or at low computational cost is an area of continued research. Rogers and Agnes [19] proposed a finite element method with altered shape functions that required fewer elements when compared to conventional finite element models. The modeling was limited, however, to the axisymmetric bimorph type mirrors and thus was not readily adaptable to the unimorph construction. Simplified analytic modeling applicable for general beam-string (a 1-D plate membrane) and axisymmetric plate membranes actuated by embedded actuators was recently presented by Shepherd et al. [20]. However, high-fidelity modeling for nonaxisymmetric systems still requires using conventional finite element methods.

In this work the AFIT deformable mirror test bed is used to study the closed-loop surface control of micron-order deformations using unimorph actuators and optical sensors. The experimental setup from the previous work is reviewed and then modeling efforts using conventional finite element techniques are presented. The results of the model are then used to create a closed-loop controller. The quasi-static control setup including experimental closed-loop results obtained and conclusions drawn from the testing completes this investigation. These results represent an incremental step toward demonstrating the technical viability of the system depicted back in Fig. 1.

III. Experimental Test Setup

A flat circular unimorph in-plane actuated tensioned membrane mirror with piezoelectric actuators was constructed for the experimental testing. The mirror properties were characterized using manufacturer data, direct measurement, and the use of a laser vibrometer for frequency analysis.

Surface deflections were measured using a Wavescope Shack–Hartmann wave front sensor with a laser operating at $\lambda = 633$ nm. For the purpose of this document one wave of light corresponds to 633 nm and the term *wavelength level* is based on this quantity. *Optical quality* then further characterizes the degree necessary to preserve an individual wavelength of light that is reflected or measured. Based upon the chosen wavelength of 633 nm, optical quality is herein defined as deflections, aberations, or scales on the order of 10's of nanometers or less.

After making optical quality measurements of the mirror's surface, the output of the Shack–Hartmann sensor is converted from slope data to an output basis set of 42 Zernike coefficients. The control signals were generated in Matlab/Simulink and implemented using dSPACE to command seven power amplifiers. Figure 3 shows an overview of the experimental setup. A more detailed description of the test setup follows.

A. Test Article

The manufacture of a flat circular unimorph in-plane actuated tensioned membrane mirror was covered in detail by Sobers et al. [18]. In summary, the mirror is a composite structure consisting of a 1.5-mm room temperature vulcanizing (RTV) silicone substrate with a coating of gold approximately 5 μm thick on the reflective side and a 52-μm PVDF actuating layer on the other. This results in a very smooth (1.7 μm peak to valley) but suboptical quality reflecting surface. A baseline shape accounting for the surface variations of up to approximately three wavelengths of light must be accounted for in the experiment. The boundary of the membrane mirror was clamped in tension in a 0.127-m diam circular aluminum ring. Although every effort was made to uniformly tension the mirror the frequency response data would later indicate a nonuniform tension field existed. This is discussed in Sec. IV.B.

An electrode pattern was etched in the bottom surface electrode to form six radial actuators and one center axisymmetric circular actuator as shown in Fig. 4. Although the electrode pattern is of a low spatial frequency on this small-scale test article, actuation electrodes of the same size applied to a large-scale space telescope mirror would

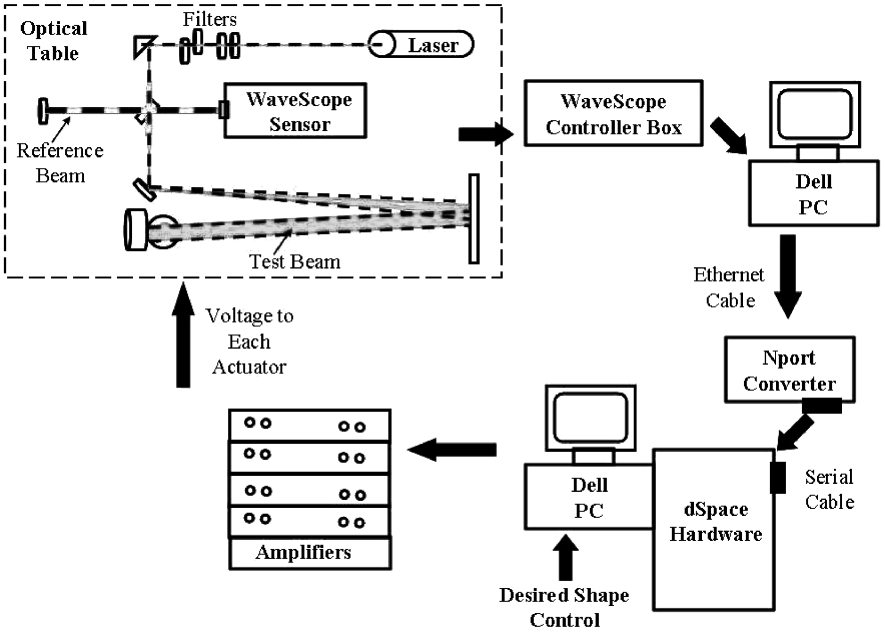

Fig. 3 Experimental test setup.

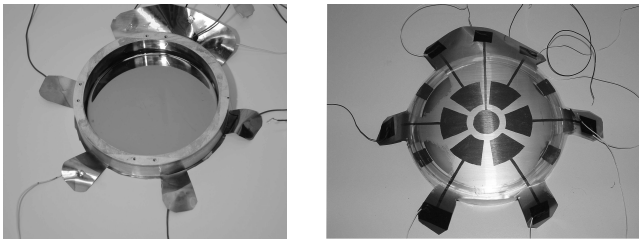

a) Reflective mirror surface **b) Piezoelectric electrode pattern on the non-reflective (back) side of the de-formable mirror**

Fig. 4 AFIT 0.127-m diam deformable mirror.

yield a higher spatial frequency proportional to the increase in radius. The PVDF material was nonorthotropic in nature, as the strength of the piezoelectric coefficient in the y direction was over 7 times the strength of the coefficient in the x direction. The PVDF actuators were capable of being energized individually or in any combination with static and dynamic potentials of up to ± 600 V.

Rather than bonding leading directly to the deformable mirror's etched actuator patches, thin hand etched electrodes of approximately 3 mm in width were run to the boundary where the leads were attached. The actuation effects of these small electrode traces were neglected for modeling purposes. The dimensions for the actuators are presented in Table 1. The material properties are explicitly stated in Tables 2 and 3.

B. Mirror Surface Measurement

A Shack–Hartmann optics-based system was used in this experiment to provide surface measurements to the controller as depicted in Fig. 3. The optical table housing the test article and sensor was designed to reduce external vibrations and was presented in the earlier work by Sobers et al. [18]. The optical table floats on four air-isolation legs and has a Plexiglass cover to attenuate airborne disturbances such as acoustic noise and air currents. A 20-mW helium-neon laser ($\lambda = 633$ nm) was used to illuminate the deformable mirror test article and reference mirror via a beam splitter. The mirror was tested while in a horizontal position on the optics table to allow the membrane surface to articulate freely, constrained only by the clamped frame boundary condition (see Fig. 5). Light entering the WaveScope passes through a monolithic lenslet module (MLM) that focuses the light onto an RS-170v monochrome Shack–Hartmann wave front sensor. The fidelity of the data collected using the WaveScope depends on both the size and number of the lenslets in the MLM.

The data were acquired over a limited portion of the mirror's surface, consisting of an approximate 0.0381-m diam circular region centered on the mirror. For the purposes of this paper this observable region is called the mirror's *clear aperture*. This clear aperture region is depicted in Fig. 6a as the area inside the shaded region at the 0.0381-m radius. The dimensions from Table 1 are also depicted on

Table 1 Deformable mirror dimensions

Radius (mirror)	0.0635 m
Radius (center actuator)	0.0127 m
Inner radius (actuators 2–7)	0.0190 m
Outer radius (actuators 2–7)	0.0444 m
Arc length (actuators 2–7)	50 deg

Table 2 GE silicone RTV615 material properties

Parameter	Value[a]	Units
Thickness	0.0015	m
Young's modulus	1.013	10^6 N/m^2
Poisson's ratio[b]	0.497	——
Density	1020	kg/m^3
Shrinkage	0.2%	——
Applicable temperature range	−60–204	°C

[a]Anon., GE Silicones RTV615 Clear General Purpose Potting/ Encapsulating Compound, MatWeb, http:www.matweb.com [retrieved 4 May 2007].
[b]The value for Poisson's ratio was experimentally determined.

Table 3 PVDF film properties

Parameter	Value [21]	Units
Thickness	52	micron, 10^{-6} m
In-plane piezoelectric constant (d_{31})	3	10^{-12} $\frac{\text{m/m}}{\text{V/m}}$ or $\frac{\text{C/m}^2}{\text{N/m}^2}$
In-plane piezoelectric constant (d_{32})	23	10^{-12} $\frac{\text{m/m}}{\text{V/m}}$ or $\frac{\text{C/m}^2}{\text{N/m}^2}$
Young's modulus	2000–4000	10^6 N/m^2
Density	1780	kg/m^3
Applicable temperature range	−40–100	°C

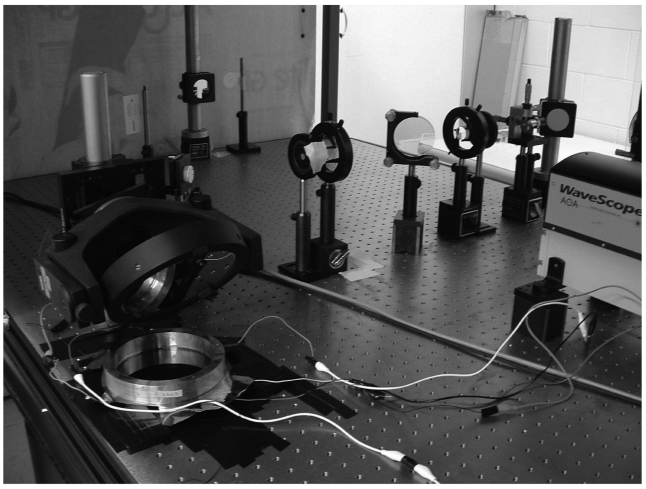

Fig. 5 Mirror (bottom left) with Shack–Hartmann measurement equipment.

the figure. These are the dimensions from which a finite element model will be constructed in Sec. IV. The mesh of the finite element model is shown in Fig. 6b.

The WaveScope sensor sends surface data to a video frame grabber in a personal computer. When performing calibration, laser returns are reflected off of the deformable mirror test article and reference mirror into the Shack–Hartmann sensor. Regions of the lenslet array which do not receive bright enough returns to provide accurate measurements (corresponding to imperfections in the mirror surface) are automatically discarded from the collected data. A minimum valid rate of 70% of the total measured subapertures was achieved for all tests. Images from the Shack–Hartmann sensor are shown in Fig. 6. Figure 6c shows an unprocessed intensity image of the mirror surface under maximum laser illumination. The interference pattern indicates a mirror surface roughness of several wavelengths of light, with evidence of printthrough of the actuator pattern. The dark areas correspond to less-reflective regions that were later not measured by the Shack–Hartmann wave front sensor, as indicated by missing subapertures regions shown in Fig. 6d. The peak-to-valley surface roughness for measured areas by the Shack–Hartmann sensor was determined to 1.7 μm, or approximately three wavelengths of the measurement system. Research to improve the surface smoothness and reduce printthrough is ongoing.

The wave front path differences of these valid data points are fitted with a WaveScope proprietary algorithm. The algorithm calculates, displays, and exports up to 42 Zernike coefficients of progressively higher order to represent the illuminated surface. The Zernike polynomials efficiently describe classical aberrations for a circular aperture of unit radius, the linear combination of which represents the surface deflection. Use of the Zernike basis set for optical applications was popularized by Noll [22] and a description of the terms is available in any introductory optics textbook.

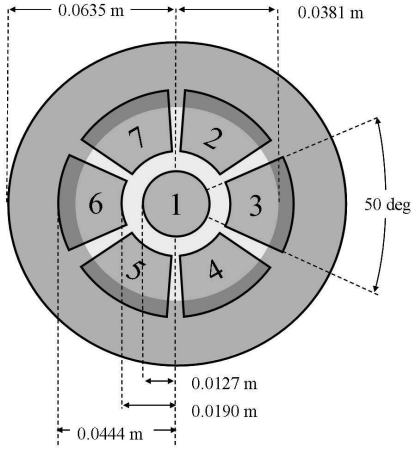

a) Dimensions of deformable mirror showing actuator numbering and the measurable area of the Shack-Hartmann sensor within a 0.0381 m radius

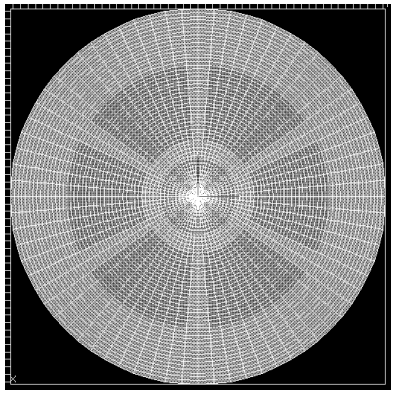

b) Finite element mesh of 3- and 4-node plate elements introduced in Sec. IV

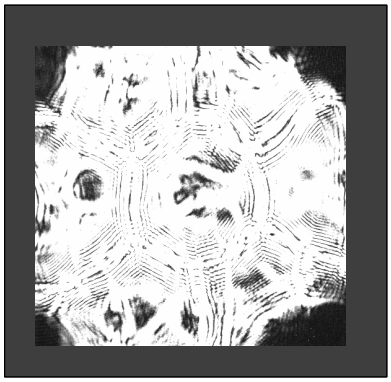

c) Mirror surface clear aperture region at maximum laser illumination level.

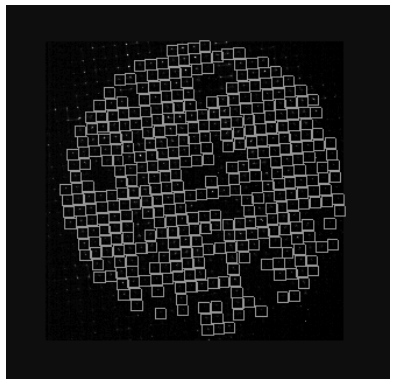

d) Typical grid depicting 370/450 of available subapertures used by the Shack-Hartmann sensor. The measured area corresponds to the 0.0381m radius in (a)

Fig. 6 Deformable mirror dimensions, modeling, and measurement.

Zernike coefficient values were updated at a maximum rate of 400 Hz from the WaveScope system but data transfer and integration with the dSPACE controller limited experimental results to 2.5 Hz. Thus some open-loop qualitative observations could be made at the higher frequency but closed-loop analysis was limited to quasi-static results within the clear aperture.

C. Closed Loop

Zernike coefficients calculated by the Wavescope sensor were exported across an ethernet cable to an NPort ethernet-to-serial converter at the 2.5 Hz rate. The serial cable is connected to the dSPACE hardware interface board. The dSPACE and second PC receive and store the data, implement real-time control through a Simulink model and Control Desktop software, and output seven control voltages to four Trek PZD 700 dual channel amplifiers. The loop is completed as each amplifier powers its respective actuator to deform the test article's mirror surface. The development of the influence function matrix using a finite element model is described next in Sec. IV followed by the control algorithm description in Sec. V.

IV. Nonlinear MSC.Nastran Finite Element Model

A differential equation for the isotropic in-plane actuated plate membrane was introduced as Eq. (1). This simplified system is valid and useful to gain insight into the behavior of the system but not accurate enough for precision control used in subsequent sections. To refine the model the analysis must be expanded to include a nonisotropic layered composite, with directional piezoelectric constants in the piezoelectric layer. Equation (1) rapidly becomes a cumbersome series of five nonlinear coupled partial differential equations for which a tractable analytic solution is nonexistent.

A model was therefore created in MSC.Nastran based on the piezoelectric-thermal analogy and was compared to test data. To create a mesh the circular domain was uniformly divided with 100 equally spaced radial divisions and 72 azimuthal divisions resulting in 7201 nodes. The spoke pattern resulted in 7128 4-node elements and 72 3-node elements. Two-dimensional plate elements were chosen over solid elements to avoid ill conditioning that can be expected when using 3-dimensional elements for problems where a single dimension is far smaller than the other two. The plate elements chosen (CQUAD4 and CTRIA3) support in-plane, bending, and transverse shear. The silicone substrate and PVDF layer were modeled using a composite element structure which derived equivalent membrane, bending, coupling, and transverse shear from each layer's physical properties as given in Tables 2 and 3.

A. Piezoelectric-Thermal Analogy

The PVDF material was modeled using a thermal expansion coefficient in accordance with the familiar piezoelectric-thermal analogy first popularized by Tiersten [23]. Use of the piezoelectric-thermal analogy to incorporate piezoelectric finite elements was reported by Babuska in an AIAA conference paper in 1997 [24]. Cote and researchers from Université de Sherbrooke, Canada, outlined the identical method updated with a more recent MSC.Nastran nomenclature [25], briefly summarized as follows:

Hooke's law with thermal strain effects (but without piezoelectric effects) may be found in any fundamental elasticity textbook as

$$\{\tau\} = [c^E](\{S\} - \{\alpha\}\Delta T) \tag{3}$$

where α_i are the thermal expansion coefficients and $\Delta T = T - T_0$ represents the change in temperature from an initial temperature. Using the piezoelectric-thermal analogy, Eq. (3) can be written in terms of the piezoelectric coupling coefficient matrix and electric field vector as

$$\{\tau\} = [c^E](\{S\} - [d]^T\{E\}) \tag{4}$$

or written in terms of the applied voltage V_i and actuator thickness t as

$$\{\tau\} = [c^E]\left(\{S\} - [d]^T\frac{1}{t}\{V\}\right) \tag{5}$$

If the simplifying assumption is made that only the out-of-plane voltage is considered (i.e., the voltage across the electrodes, V_3) and in-plane voltages are considered negligible and ignored ($V_1 = V_2 = 0$), the piezoelectric terms in Eq. (5) reduce to the result of Cote's derivation for the piezoelectric-thermal analogy:

$$\frac{d_{31}}{t}V_3 = \alpha_1\Delta T \tag{6}$$

$$\frac{d_{32}}{t}V_3 = \alpha_2\Delta T \tag{7}$$

Thus for the problem herein the active elements were given x and y coefficients for planar thermal expansion in their piezoelectric layer using the values from Table 3 and are shown in Fig. 6b. All other regions, plus the silicone substrate, were left thermally inert. Voltage was then applied as an equivalent temperature to the nodes of the corresponding actuators.

B. Modeling Edge Tension

When the deformable mirror was constructed a suitable method of measuring and recording edge tension was not available. Although presumably the edge tension would be available for a commercially manufactured mirror, due to the handmade nature of the test article, an alternate method to determine the pellicle tension field was required. It was decided to perform a dynamic analysis of the test article and then implement a tension field in the finite element model that would approximate the frequency and mode shapes for the first six recorded modes. A laser vibrometer was used to scan the surface of the mirror when excited by chirp signals produced by an air horn using 50–100 Hz and 100–250 Hz frequency ranges. Upon post data analysis it was determined that mode 2 (the eigenvector pair to mode 3 for a traditional membrane) was not observed in the measured data set, possibly attributable to the use of two different excitation methods near the modal frequency.

The natural frequency data and eigenvector data did not match the membrane theoretical solution for a circular boundary because of an apparent asymmetry in the tension field despite best efforts to maintain symmetry when the mirror was constructed. Although a matching algorithm could likely prescribe a set of nodal forces to exactly match the observed eigenvalue/eigenvector pairs it was hypothesized that a perturbed elliptic tension field could provide satisfactory results without unnecessarily complicating the model. The motivation for selecting an elliptical field was that the membrane was stretched over its supporting boundary frame by two laboratory technicians each simultaneously stretching the membrane material perpendicular to the other while working around the frame in small increments. Presuming the two tension fields applied by the technicians were not equal, it was assumed the field would have a major and a minor axis.

To implement the proposed membrane elliptical strain field the tension (N) was implemented with a tangential force along the boundary governed by the three parameter equation:

$$N(R,\theta) = \varrho(1 + \varepsilon\cos^2(\theta - \theta_0)) \tag{8}$$

To match the laser vibrometer modal data for the deformable mirror the parameters ϱ, ε, and θ_0 were chosen using an empirical comparison of the eigenvectors as depicted in Fig. 7. The θ_0 coordinate served to align the orientation of the tension field in the finite element model to that of the experimental data and the remaining two parameters were used to adjust the tension field such that the eigenvalue frequencies of the finite element model matched the two lowest experimentally observed modes (modes 1 and 3). The values of $\varrho = 170$ N/m, $\varepsilon = 0.784$, and an orientation of $\theta_0 = 105$ deg were programmed in the model and then solved using the linear modal analysis solution (SOL 103). The agreement between

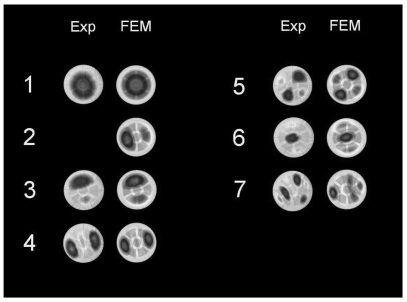

Fig. 7 Eigenvector comparison between experimentally obtained laser vibrometer mode shapes and the finite element model after application of a prescribed tension field boundary condition.

the experimentally obtained modal data and the finite element model achieved using the proposed strain field is shown in Fig. 7 and Table 4. Also included in Table 4 are the eigenvalues from membrane theory of a symmetrically tensioned circular membrane normalized to the fundamental mode shape, available from a number of introductory texts on continuous dynamics and vibration.

C. MSC.Nastran Solution Strategy

Linear solutions to the finite element model as presented cannot accurately represent the surface deflections of the physical structure. This is because the stiffening effect of the membrane tension from the boundary loading conditions is not present—the linear solution is the independent combination of the linear stretching (resulting in constant surface deflections removed as a bias) and piezoelectric actuation of the nontensioned plate (greatly exaggerating the surface deflection due to the weak contribution of the plate's flexural rigidity). Therefore, a nonlinear solution is required.

A nonlinear static solution was obtained using the MSC.Nastran proprietary algorithm. The edge load (or tension) was applied in 10 increments. Within each load increment a modified Newton–Raphson approach, the BFGS method (Broyden–Fletcher–Goldfarb–Shannon) was used to resolve a form of a tangential stiffness matrix. In this manner membrane tension resulted in a geometric stiffening of the structure. Difficulties in convergence due to singularities caused by high membrane-to-bending stiffness ratios, evident when using nonlinear solution techniques, were overcome by introducing an incremental stiffness on the drilling degrees of freedom [26] (in MSC.Nastran this technique is implemented with the K6ROT card). After the membrane tension was introduced a second subcase generates the piezoelectric load through an equivalent thermal load as previously described.

Experimental data are compared to the static finite element solution in Fig. 8. A voltage was individually applied to each of three separate actuators, resulting in the displacements as shown in the figure. The experimental surface was obtained from a linear combination of 42 Zernike basis functions that were averaged over approximately 80 consecutive measurements.

Next, a baseline (0-volt) surface was subtracted from each plot to remove any initial surface deflection (a resting surface deflection or roughness of 1.7 μm peak to valley was observed). For the finite element solution, displacements in the vertical (z axis) direction were

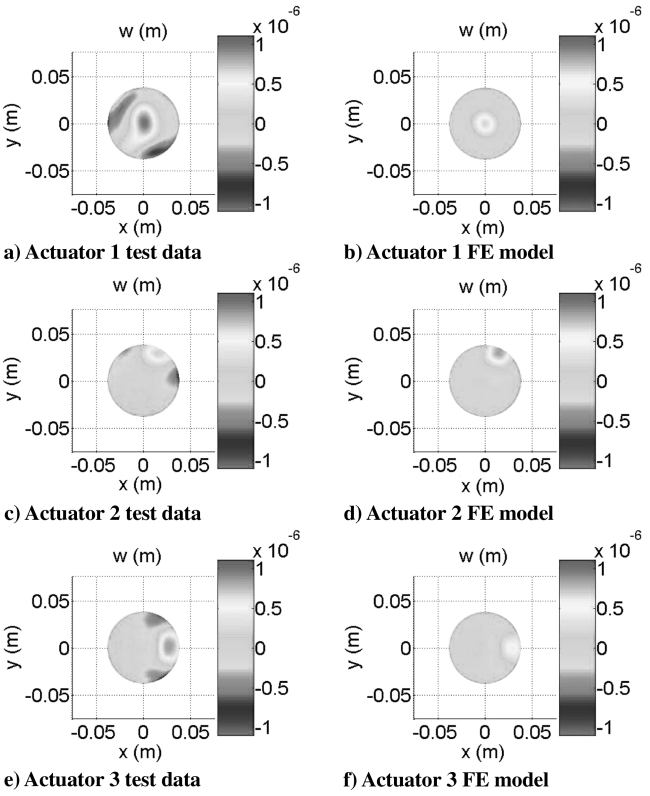

Fig. 8 Representation of the static deflections as a summation of 42 Zernike modes.

recorded and then a surface was determined from the linear combination of the same 42 Zernike basis functions as fit to the data. Reporting the surface deflection in terms of a limited number of Zernike basis functions, as is common for many optical measurement systems, necessarily filters the data. For the experimental data the smoothing effect was a consequence of the Shack–Hartmann slope measurement technique, number of subapertures chosen, and the fitting algorithm. For consistency the MSC.Nastran results are reported using the same basis elements (Zernikes), which enables a direct comparison between the experimental and finite element data inside the clear aperture. The *unfiltered* MSC.Nastran data would show slightly sharper edges along the boundary of the actuators, but is considered of negligible impact for this case. An analysis of the surface displacement in these regions as a function of the mirror parameters is the subject of the presentation by Shepherd et al. [20]. Thus the surface displacement as a summation of the first 42 Zernike basis functions such as output by the Wavescope software is presented in Fig. 8.

V. Quasi-Static Surface Control

The controller for this system was created imposing several constraints. First, the controller was built without any calibration data

Table 4 Modal frequency comparison (Hz)

Mode	Experimental	Membrane theory[a]	Error[b]	Finite element	Error[b]
1	76	76	0.0%	76	0.0%
2[c]	——	121		116	
3	129	121	−6.2%	129	0.0%
4	146	162	11.0%	155	6.1%
5	163	162	−0.6%	165	1.2%
6	188	174	−7.4%	186	−1.1%
7	228	202	−11.4%	198	−13.2%

[a]The frequencies for membrane theory were normalized to the first observed experimental modal frequency.
[b]Relative % error as compared to experimental value.
[c]The second modal frequency was not measured in the experimental test data.

(that is without any a priori knowledge of the WaveScope measurements). For some applications it may prove easier to control the system by applying demonstrated system identification techniques; however, the objective of the work herein is to demonstrate that the existing finite element theory was sufficient for modeling and controlling this class of structure. Second, the hardware and software used had both a limited data rate and a limited number of control outputs. Given these constraints, quasi-static surface control was achieved for this class of mirror with the controller as outlined in the following paragraphs.

Conventional techniques were employed to construct a controller for the system. The controller used proportional plus integral control which consisted of a static gain matrix, a bank of antiwindup integrators, and a smoothing filter. The "antiwindup" refers to the fact that the integral action is turned off whenever the actuators saturate. Rate transition filters were used to match the control input calculations with the measurement rate. An overview of the controller implementation is shown in Fig. 9, followed by a discussion of the controller components.

A. Static Gain Matrix

A static gain matrix K was formed using static Zernike representations of surfaces formed from the MSC.Nastran finite element model. The static shapes represented by the 42 Zernike coefficients were created for each of the seven actuators and normalized to a 1 V application. Each 42-element vector was placed in a matrix Y. Thus the static system was

$$[A]_{42\times7}[X]_{7\times7} = [Y]_{42\times7} \tag{9}$$

where A was the unknown system and X was an identity 7×7 matrix corresponding to the 1 V application to each of the actuators. Trivially, $A = Y$. For the control problem where a desired surface z of up to 42 Zernike coefficients is desired, the problem to be solved is

$$[A]_{42\times7}\{v\}_{7\times1} = \{z\}_{42\times1} \tag{10}$$

where v represents the control voltage inputs. Or simply, we require

$$\{v\} = [K]\{z\} \tag{11}$$

where K is determined using

$$[K] \equiv [([A]^T[A])^{-1}[A]^T]_{7\times42} \tag{12}$$

The solution (a pseudoinverse) represents the minimum 2-norm solution to Eq. (9). For this system, where discontinuous actuators have nonoverlapping surface displacement functions, the inverse will exist. Increased actuator densities, however, may require alternatives to Eq. (12) in cases where the surface displacement functions of the actuators intersect.

The gain matrix K acted on the error signal in the feedback path as shown in Fig. 9 where the error signal is defined as

$$\{z\} \equiv \{z_e\} = \{z_{\text{desired}}\} - \{z_{\text{measured}}\} \tag{13}$$

B. Proportional Plus Integral Control

Once the appropriate gains were calculated by multiplication of the gain matrix with the error signal, the resulting voltages were immediately applied, plus stored in a bank of antiwindup integrators for use in the next time step. Antiwindup integrators were used to reduce the lag from a buildup of error in cases where the input signal exceeded the physical capacity of the system (that is, outside of the controllable space). An antiwindup integrator is exactly the same as a traditional integrator except that when the input reaches a specified threshold value the antiwindup integrator suspends its summation until the input value returns into the allowable range. The antiwindup integrators had cutoffs set at ± 600 V corresponding to the saturation limits of the amplifiers. Further input protection (not shown) was also included in a saturation block just before the input to the amplifiers. Without the antiwindup feature, a built-up error would sum continuously and cause unacceptable lags in the controller.

C. Integration

The controller operated at 2.5 Hz, consistent with the measurement rate of the WaveScope sensor system. The Simulink/dSPACE controller was operated at a much higher frequency and thus had to be stepped down in frequency through rate transition blocks before entering the control and stepped up upon leaving the controller.

Open-loop testing, where higher frequency measurements could be qualitatively observed, showed considerable "ringing" of the mirror if the 2.5 Hz step inputs were applied to the actuators. The

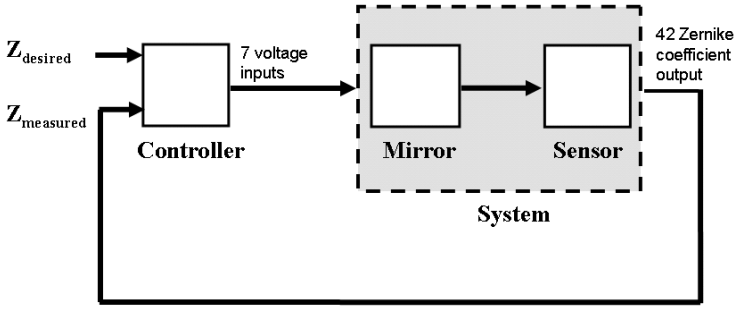

a) System overview operating at 11 KHz

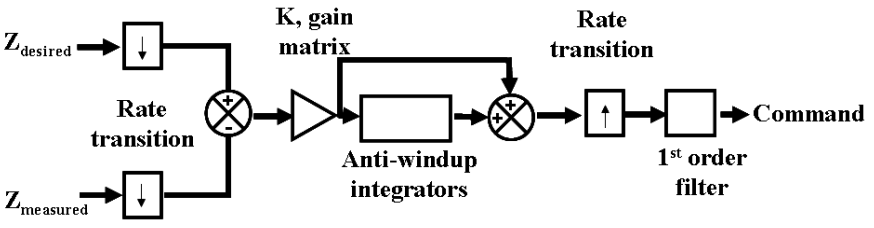

b) The "Controller" of (a) operates at 2.5 Hz (consistent with the measurement rate) on an error signal consisting of a static gain matrix and antiwindup integrators. The control output is filtered to prevent "ringing" the mirror

Fig. 9 Block diagram of system as implemented in Simulink software.

ringing could not be observed at the slow measurement speed in the closed-loop testing; however, a first-order filter with a 2.5 Hz cutoff frequency was installed after the rate transition block to the higher system frequency. This was used to smooth the control input to the amplifiers and theoretically lessen the excitation of the mirror dynamics.

Because of processing limitations only a limited number of the available outputs (that is, Zernike coefficients) could be recorded. Thus, although the controller minimized the error for all 42 Zernike commanded inputs, only a subset of signals were used. For the testing presented in this document the retained measurements were the Zernike coefficients for tip, tilt, and defocus.

VI. Experimental Testing and Results

A series of quasi-static tracking tests were run to demonstrate the effectiveness of the in-plane actuated tensioned deformable membrane mirror under the control of a purely theoretically developed controller using standard finite element modeling and control practices.

Measurements were limited to tip, tilt, and defocus Zernike coefficients within the mirror's clear aperture. Although the telescope designer is typically concerned with the quality of the higher-order Zernike coefficients, the low modes chosen were deemed adequate when considering the size of our test mirror. The objective of this test is to demonstrate the closed-loop performance of the in-plane actuated membrane mirror, and for this purpose, control of the low-order modes is sufficient. The low-order modes have the advantage of being intuitively recognizable, controllable with a low density actuator setup, and measurable with the Shack–Hartmann wave front sensor. Also, as previously noted, an actuator grid composed of the same sized electrode elements on a large-scale mirror would yield a much higher actuator spatial frequency. From Eqs. (1) and (2) there is nothing to prevent one from inferring (in a linear sense) that results achieved on controlling low-order Zernike modes with the low spatial frequency actuator pattern on the small-scale test article could not be achieved on higher-order Zernike modes on the large-scale mirror with its increased spatial frequency.

In the testing that followed, an open-loop baseline signal (or bias) was subtracted from each Zernike coefficient before each closed-loop test (on the order of 1–10 μm for the tip, tilt, and defocus Zernike). Given the nature of the test setup (where small thermal or other variations of the platform could slightly affect the beam path) it was not uncommon for a bias of approximately 0.3 μm to reappear upon test completion (after a period of minutes) in the defocus Zernike modes, and it is assumed that the control results presented also had to overcome these small biases as well.

The deformable mirror controller was run in two test configurations as indicated in Table 5. In the first configuration the measurement of the defocus Zernike was the single output used to create an error signal. A sinusoidal command signal of 1.0 μm in amplitude at a 0.04 Hz was input into the controller while the other 41 Zernike coefficients were commanded to zero. The amplitude was statically obtainable by the mirror and the frequency was well below both the dynamic modes of the mirror and the measurement update rate of 2.5 Hz. Next, the amplitude was increased to 2.0 μm, exceeding the mechanical limits of the mirror, to test the effectiveness of the antiwindup integrators.

In test 2 three outputs of the mirror were tracked simultaneously. The chosen outputs were tip, tilt, and defocus. The tracking signal shown in Table 5 commanded the tip Zernike at 0.02 Hz at 0.6 μm in amplitude and the focus Zernike at 0.04 Hz at 1.0 μm, while commanding the tilt Zernike (and the remaining 39 other Zernikes) to zero.

The average absolute error for each test is presented in Table 6. The average absolute error was the absolute value of the command signal versus the measured coefficient taken pointwise at the sample rate, summed over the measurement period, and then divided by the total number of points. In test 1b the procedure was modified such that when the command signal exceeded 1.0 μm (when the command was outside of the controllable space) the measurement was compared against a reference of 1.0 μm. The test results are further discussed in the following sections.

A. Single Zernike Measurement Tracking

The test results for the single measurement tracking are shown in Fig. 10. For the first tracking test of the defocus Zernike the signal is within an absolute error of 0.16 μm. The results indicate tracking precision bordering on (within an order of magnitude of) optical quality. The results show the existence of sharp, oscillatory behavior which may be attributed to two possible factors: 1) system dynamics could be excited and aliased into the measurements, or 2) the measurement noise (amplified through the system gain) also affected the results. The behavior was present in all subsequent tests and was independent of input signal amplitude. The impact of system dynamics (traditional membrane behavior) must be addressed in future constructs as large membrane telescope mirrors will have resonant modes at lower frequencies inversely proportional to their radius.

The measurement noise was considered a significant factor only in measuring the defocus Zernike mode (tip and tilt modes were negligibly affected by noise). Calibration tests against static solid plate mirrors could be achieved with optical quality accuracy only when a bias in the defocus mode was removed. Stated another way, the defocus Zernike mode of the measurement system would slowly vary (variations of approximately 0.3 μm with time constants on the order of several minutes) but could be tracked cleanly with a tolerance of approximately 10 nm by the Wavescope system. This variance was attributed to changes in the beam path length and is a

Table 5 Test matrix

Test	Commanded Zernike	Signal, m	Zernike polynomial
1a	Defocus	$1.0 \times 10^{-6} \sin(2\pi 0.04t)$	$\sqrt{3}(2r^2 - 1)$
1b	Defocus	$2.0 \times 10^{-6} \sin(2\pi 0.04t)$	$\sqrt{3}(2r^2 - 1)$
2	$\left\{\begin{array}{c}\text{tip}\\ \text{tilt}\\ \text{defocus}\end{array}\right\}$	$\left\{\begin{array}{c}0.6 \times 10^{-6} \sin(2\pi 0.02t + \frac{\pi}{2})\\ 0.0\\ 1.0 \times 10^{-6} \sin(2\pi 0.04t)\end{array}\right\}$	$\left\{\begin{array}{c}2r\cos\theta\\ 2r\sin\theta\\ \sqrt{3}(2r^2 - 1)\end{array}\right\}$

Table 6 Average absolute value of error signal

Test	Zernike coefficient	Average error, m	Comments
1a	Defocus	0.16×10^{-6}	——
1b	Defocus	0.31×10^{-6}	Note error for command outside of controllable space measured vs 1.0×10^{-6}
2	$\left\{\begin{array}{c}\text{tip}\\ \text{tilt}\\ \text{defocus}\end{array}\right\}$	$\left\{\begin{array}{c}0.14 \times 10^{-6}\\ 0.09 \times 10^{-6}\\ 0.18 \times 10^{-6}\end{array}\right\}$	——

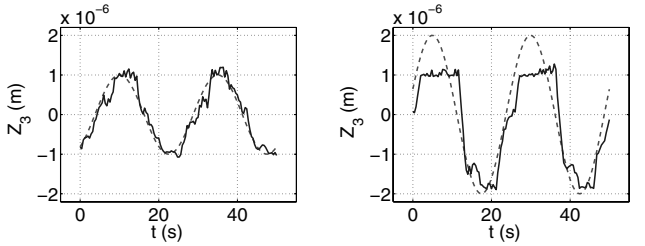

a) Tracking defocus Zernike

b) Tracking defocus Zernike with amplitude in excess of controllable limit

Fig. 10 Experimental test 1 data. The dashed lines indicate the command inputs; the solid lines are the closed-loop mirror responses.

reason that the defocus mode is often corrected in optical systems. As the defocus error was used directly in the control system signal the ultimate impact of the defocus bias error was small and does not affect the validity of the results presented.

Next, the amplitude of the commanded signal was increased to test the effectiveness of the antiwindup integrators. Clearly, the antiwindup integrators performed and did not allow a build of error to prevent signal tracking. However, the nonsymmetric nature of response warrants a comment. The system responded with a maximum positive deflection of 1 μm, and a maximum negative deflection of 1.8 μm. This could be attributed to bias uncertainties and drift in the beam path not removed before the closed-loop test, or attributed to anisotropic material properties, and remains open for future investigation. Another observation was the apparent lag in the response when deflections at the actuation limit were made. For this type of mirror construction it is possible that hysteretic effects may be present attributable not only to the piezoelectric actuators but potentially due to the silicone substrate strain-rate effects typical of viscoelastic materials. System lags will need to be measured and quantified for use with higher bandwidth applications.

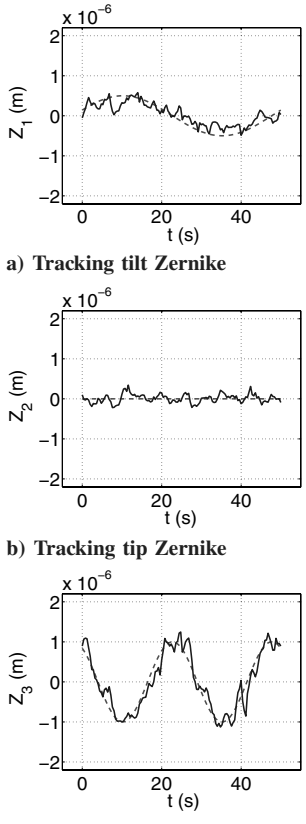

a) Tracking tilt Zernike

b) Tracking tip Zernike

c) Tracking defocus Zernike

Fig. 11 Experimental test 2 data recorded simultaneously. The dashed lines indicate the command inputs and the solid lines are the closed-loop mirror responses.

B. Multiple Zernike Measurement Tracking

The results of the previous section demonstrated a single Zernike mode could be tracked, but no mention was made of the effect on the other optical modes. In the second test shown in Table 5, three Zernike modes were commanded and the tracking results are shown in Fig. 11.

As was the case presented in Sec. VI.A, the closed-loop system was able to track multiple inputs with a maximum error of 0.18 μm. Another important conclusion was that tracking tip and tilt modes did not significantly detract from the tracking of the defocus Zernike. These results were consistent for various input amplitudes provided the commands were within actuator stroke limitations.

Postexperiment analysis was conducted using the linear model derived from the finite element results [the [*A*] matrix from Eq. (10)]. Application of a preconditioning nonlinear hysteresis model to the input voltages, and the addition of measurement noise to the Zernike outputs, were used in the simulation. The results were qualitatively similar to the experimental testing. Characterization of both the hysteresis and measurement is ongoing and will be reported separately. It is noted that system noise and nonlinear effects such as hysteresis will govern the ultimate performance of the deformable mirror especially for higher temporal frequency (non-quasi-static) applications. Construction and testing of mirrors with higher actuator densities are in process and will be reported on in the future.

VII. Conclusions

The results presented herein represent a quasi-static control experiment for the in-plane piezoelectric-actuated deformable membrane mirror. Simultaneous tracking of tip, tilt, and defocus modes within a fixed boundary support illustrate the potential of this class of mirror to control independent Zernike modes with accuracy approaching that required of an optical system. The performance was potentially hindered by high frequency membrane dynamics aliased into the optics-based control system, measurement noise, and nonlinear material effects. These concerns remain a item of ongoing research.

When considering a simplified governing differential equation, the results suggest control of higher-order Zernike modes of increased spatial frequency would be possible for a large-scale mirror with its corresponding increased actuator density. For control, a prescriptive technique for modeling a tensioned deformable mirror with in-plane actuators using available nonlinear finite element modeling software was given. Results demonstrate that the analytical model was adequate for producing the actuator influence matrix used in the proportional plus integral control scheme. This has clear advantages to the space application envisioned where detailed in situ calibration data may be difficult if not impossible to obtain.

The success of this experimental demonstration illustrates the potential of unimorph in-plane actuation for the quasi-static control of deformable membrane mirrors. Yet to be demonstrated, however, are the large deflections (on the order of centimeters) necessary for a large-scale reflector. Linear analysis of governing differential equations may indicate increases in the strength of the piezoelectric coefficients or decreases in membrane tension would achieve a greater magnitude of surface deformations and provide a path for future exploration. Manufacturing techniques are required so that surface smoothness is improved to optical quality while at the same time reducing edge tension. Lastly, as envisioned for the space telescope application, a combination of precision boundary control (such as presented by Patrick et al. [7]) with in-plane actuation as described herein, has a significant potential to achieve the overall desired weight savings and dynamic optical performance desired for future space-based telescopes.

Acknowledgments

The research presented in this document was conducted with the financial support of the U.S. Air Force Office of Scientific Research

under the direction of Lieutenant Colonel Sharon Heise. The authors would like to thank the editor and the reviewers for their dedication to improving the quality of the material presented. Their insightful comments served not only to improve the readability of the text but stimulated many other avenues for the research and thus we offer our sincerest gratitude.

References

[1] Marker, D., and Jenkins, C., "Surface Precesion of Optical Membranes with Curvature," *Optics Express*, Vol. 1, No. 11, 1997, pp. 324–331.

[2] Bekey, I., "A 25 M. Diameter Space Telescope Weighing Less Than 150 Kg," AIAA Paper 1999-4478, 1999.

[3] Moore, J., Patrick, B., Gierow, P., and Troy, E., "Design, Test, and Evaluation of an Electrostatically Figured Membrane Mirror," *UV/Optical/IR Space Telescopes: Innovative Technologies and Concepts*, edited by H. MacEwen, SPIE, Bellingham, WA, 2004, pp. 188–196.

[4] Malin, M., Macy, W., and Ferguson, G., *Edge Actutation for Figure Control*, Vol. 365, SPIE, Bellingham, WA, 1982, pp. 114–122.

[5] Nichols, J., Duneman, D., and Jasso, J., "Performance Evaluation of an Edge-Actuated, Modal, Deformable Mirror," *Optical Engineering*, Vol. 22, No. 3, 1983, pp. 366–370.

[6] Lindler, J., and Flint, E., "Boundary Actuation Shape Control Strategies for Thin Film Single Surface Shells," AIAA Paper 2004-1825, 2004.

[7] Patrick, B., Moore, J., Chodimella, S., Marker, D., and deBlonk, B., "Final Testing and Evaluation of a Meter-Class Actively Controlled Membrane Mirror," *47th AIAA/ASME/ASCE/AHS/ASC Structures, Structural Dynamics and Materials Conference*, AIAA, Reston, VA, 2006, pp. 3753–3765.

[8] Hubbard, J., and Burke, S., "Shape Control of Piezoelectric Bimorph Mirrors," *Analysis of Optical Structures*, edited by D. O'Shea, Vol. 1532, SPIE, Bellingham, WA, 1991, pp. 207–214.

[9] Tyson, R., *Principles of Adaptive Optics*, Academic Press, New York, 1991.

[10] Adelman, N., "Spherical Mirror with Piezoelectrically Controlled Curvature," *Applied Optics*, Vol. 16, No. 12, 1977, pp. 3075–3077.

[11] Albertinetti, N., Aldrich, R., and Everson, J., "Deformable Mirrors with Bimorph Actuators," *Adaptive Optical Components 2*, edited by S. Holly, Vol. 179, SPIE, Bellingham, WA, 1979, pp. 28–31.

[12] Agnes, G., and Wagner, J., "Adaptive Structures Technology for Membrane Optical Surfaces," AIAA Paper 2001-1199, 2001.

[13] Yang, E., Dekany, R., and Padin, S., "Design and Fabrication of a Large Vertical Travel Silicon Inchworm Microactuator for the Advanced Segmented Silicon Space Telescope," National Aeronautics and Space Administration, TR 02-3144, 2002.

[14] Açikmeşe, A., Mettler, E., Breckenridge, W., Macenka, S., and Tubbs, E., "L2 Earth Atmosphere Observatory: Formation Guidance, Metrology, and Control Synthesis," AIAA Paper 2004-5212, 2004.

[15] Nayfeh, A., and Pai, P., *Linear and Nonlinear Structural Mechanics*, Wiley Series in Nonlinear Science, Wiley-Interscience, New York, 2004.

[16] Steinhaus, E., and Lipson, S., "Bimorph Piezoelectric Flexible Mirror," *Journal Optical Society of America*, Vol. 69, No. 3, 1979, pp. 478–481.

[17] Sumali, H., Massad, J., Reu, P., Chaplya, P., and Martin, J., "Analytical and Experimental Studies of Orthotropic Corner-Supported Plates with Segmented In-Plane Actuators," *2005 ASME International Mechanical Engineering Congress and Exposition*, American Society Of Mechanical Engineers, New York, 2005.

[18] Sobers, D. M., Agnes, G. S., and Mollenhauer, D., "Smart Structures for Control of Optical Surfaces," AIAA Paper 2003-1559, 2003.

[19] Rogers, J., and Agnes, G., "Modeling Discontinuous Axisymmetric Active Optical Membranes," *Journal of Spacecraft and Rockets*, Vol. 40, No. 4, 2003, pp. 553–564.

[20] Shepherd, M. J., Cobb, R. G., and Baker, W. P., "Low-Order Actuator Influence Functions for Piezo-Electric In-Plane Actuated Tensioned Circular Deformable Mirrors," *Smart Structures and Materials 2006: Modeling, Signal Processing, and Control*, edited by D. K. Lindner, Vol. 6166, SPIE, Bellingham, WA, 2006.

[21] Anon., Piezo Film Sensors Technical Manual, Measurement Specialties, Inc. Sensor Products Division, 1999.

[22] Noll, R., "Zernike Polynomials and Atmospheric Turbulence," *Journal Optical Society of America*, Vol. 66, No. 3, 1976, pp. 207–211.

[23] Tiersten, H., *Linear Piezoelectric Plate Vibrations; Elements of the Linear Theory of Piezoelectricity and the Vibrations of Piezoelectric Plates*, Plenum Press, New York, 1969.

[24] Babuska, V., and Freed, B., "Composite Piezoelectric Beam and Plate Elements for Structural Control," *38th AIAA/ASME/ASCE/AHS/ASC Structures, Structural Dynamics, and Materials Conference and Exhibit*, AIAA, Reston, VA, 1997, pp. 1607–1620.

[25] Cote, F., Masson, P., Mrad, N., and Cotoni, V., "Dynamic and Static Modelling of Piezoelectric Composite Structures Using a Thermal Analogy With Msc/Nastran," *Composite Structures*, Vol. 65, No. 3, 2004, pp. 471–484.

[26] Lee, S., *MSC/NASTRAN Handbook for Nonlinear Analysis: based on Version 67*, MacNeal-Schwendler Corp., Los Angeles, CA, 1992.

L. Peterson
Associate Editor